Supporting Information

Mirsaidov et al. 10.1073/pnas.1200457109

SI Text

Transmission Electron Microscopy (TEM) Liquid Cell. We characterized the topography and the surface potential of freestanding Si_3N_4 membrane window prior and postglow discharge using commercial atomic force microscope (X-120; Park Systems) to match the surface properties of our conditions. The cleaning and glow discharge was similar to those of actual membranes used for study as described above. The topography in Fig. S1 *B* and *C* shows that plasma treatment does not affect surface topography of Si_3N_4 membrane and the rms roughness for untreated and glow discharged surface of freestanding Si_3N_4 membrane is about 0.5 nm. Scanning kelvin probe microscopy revealed that the surface potential of freestanding Si_3N_4 membrane postglow discharge is uniform and about 300 mV.

Droplet Formation. Water loaded into liquid cell is sandwiched between the two Si_3N_4 membranes. Exposing this water layer to intense electron flux (greater than 100 electron/(Å^2·s)) causes water to rapidly retract under the beam, leaving a thin water film (approximately 5–20 nm) behind. Recent macroscopic observations show that a small volume of water can be pushed by an electric field leaving water film behind (1), and we suspect that similar phenomenon is occurring here when water is exposed to an electron beam. The thin layer of water in our liquid cell then slowly recedes under intense electron flux as captured by series of micrographs, shown in Fig. S2. The receding water film leaves nanometer size droplets on the surface of the membrane window.

Change in the Surface Potential of the Si_3N_4 Membrane Window Due to the 120-keV Electron Beam. We measured the change in the surface potential of Si_3N_4 membrane prior and postelectron beam irradiation under the similar conditions used in our experiments (approximately 60 e/Å^2·s for approximately 4 min). Several measurements were performed within 1–2 h of irradiation. These measurements clearly indicate that the membrane potential is slightly offset (approximately 130 mV) (Fig. S3) when irradiated by electron beam. However, we do not attribute the liquid movement during dewetting to this surface modification because water starts flowing back within a few minutes and wetting the film once the beam intensity is reduced or turned off while the surface clearly remains charged, as shown in Movie S1. Therefore, we think it is the interaction between electron beam and the liquid film (possibly the voltage gradient at the edges of the film and not just a uniform offset of the membrane potential) that causes dewetting of Si_3N_4 membrane window.

Thickness Estimates. We can roughly estimate the thickness of the nanodroplet using the relative intensity of the transmitted electrons (electron count) through the droplet (N_{drop}) and through the droplet free area of the image (N_1) using

$$\frac{N_{\text{drop}}}{N_1} \approx \exp(-t_{\text{drop}}/l_{\text{water}}),$$

where t_{drop} is the thickness of the nanodroplet and l_{drop} is the mean free path for electron passing through water. The thickness is then

$$t_{\text{drop}} \approx -l_{\text{water}} \ln \frac{N_1}{N_{\text{drop}}}.$$

The images in Fig. S4 illustrate the thickness estimates of a stationary droplet and as droplet readies to take a step. The higher contrast relative to the substrate represents the thicker liquids.

It is unlikely that the change in image contrast within the droplet as it prepares to step is from nanobubbles, because liquid droplet of almost the same volume has been recovered in the following process. In addition, no other configurations have been observed, although the nucleation of a bubble within the center of the droplet is not energetically more favorable compared to the edges or off centers.

Comparison Between 30- and 60-nm Droplets. See Fig. S5.

On the Heating of the Nanodroplet Due to the Electron Beam. ***Droplet temperature.*** We would like to consider the possible effect of electron beam-induced heating of water nanodroplets because they may have an effect on dynamics of water. The energy is delivered to droplet in the form of the electron energy loss as electrons undergo inelastic scattering in water. The electron energy loss can be estimated using Bethe function (2):

$$\frac{dE}{dx} = -\frac{2\pi e^4 N_A Z \rho}{AE} \ln\left(\frac{\alpha E}{I}\right), \qquad \textbf{[S1]}$$

where E is the incident electron energy, x is distance traveled through the medium, I is estimated ionization energy, Z is atomic number of the material, e is electron charge, N_A is Avogadro's number, ρ is density of the material, A is atomic mass of the material, and the relativistic factor constant at 120 keV is $\alpha = 1.16$. Using Eq. **S1**, electron energy loss of 120 keV electrons transmitting through water and Si_3N_4 is calculated to be $dE/dx =$ 0.21 eV/nm and $dE/dx = 0.2$ eV/nm, respectively.

Next, we assume that all the electron energy loss transfers into heat and that the heat dissipation is only possible via two-dimensional thermal conduction through the thin Si_3N_4 membrane (3). Then, the temperature increase of the thin membrane can be calculated using a two-dimensional heat conduction equation and ignoring the heat loss through other mechanisms. At steady state, the two-dimensional heat conduction equation in cylindrical coordinates can be expressed as

$$-\kappa_{\text{memb}}\left(\frac{d^2T}{dr^2} + \frac{1}{r}\frac{dT}{dr}\right) = J, \qquad \textbf{[S2]}$$

where κ_{memb} is thermal conductivity of Si_3N_4 membrane, T is temperature, r is the distance to the center of heat source, and J is the heat density flux. Heat flows from the electron beam irradiated area of radius R_b to the heat sink at the edge of membrane window (Si frame of the chip at $r = R_w \approx 10$ μm–window radius) where we assume the heat sink temperature to be at ambient temperature, $T = T_0$. Outside the irradiated area ($R_b \le r \le R_w$) there is no net heat flux ($J = 0$) and the boundary conditions are $T(R_w) = T_0$ and $dT(R_b)/dr = Q/(2\pi R_b t \kappa_{\text{memb}})$, where Q is the net heat power input and t is the membrane thickness. The solution to Eq. **S2** results in the temperature expression

$$T = T_0 + \frac{Q}{2\pi\kappa_{\text{memb}} t} \ln(R_w/r). \qquad \textbf{[S3]}$$

At the boundary between the irradiated and nonirradiated area ($r = R_b$) we get

$$T_b = T(R_b) = T_0 + \frac{Q}{2\pi\kappa_{\text{memb}} t}\ln(R_w/R_b). \quad \textbf{[S4]}$$

However, within the irradiated area ($r \le R_b$), the heat flux density is $J = Q/(\pi R_b^2 t_{\text{memb}}) = n(dE/dx)$, where n is the electron flux (i.e., number of electrons arriving per unit area per unit time) and t_{memb} is the membrane thickness. In this case, the solution to Eq. **S2** yields the temperature at the illuminated area to be

$$T = T_b + \frac{1}{4\kappa_{\text{memb}}} J_{\text{memb}}({R_b}^2 - r^2). \quad \textbf{[S5]}$$

Now let us consider the droplet residing on a surface of Si_3N_4 membrane and assume that it is in the center of the irradiated area (Fig. S6) at ($r = 0$) where the membrane temperature is

$$T_{\text{memb}} = T_0 + \frac{Q}{2\pi\kappa_{\text{memb}} t}\ln(R_w/R_b) + \frac{{R_s}^2}{4\kappa_{\text{memb}}} J_{\text{memb}}. \quad \textbf{[S6]}$$

Next, we consider the droplet residing on top of this Si_3N_4 membrane (where $R_{\text{drop}} \ll R_b$). As illustrated in Fig. S6, we make an assumption that heat flows through a thin contact interface layer of thickness l_0 as drop temperature reaches T_{drop} due to heat power input, Q, from electron beam. Then, the one-dimensional heat transfer equation is given by

$$-\kappa_{\text{drop}} \frac{d^2 T}{dz^2} = 0 \quad \textbf{[S7]}$$

with the simple solution

$$T_{\text{drop}} = \frac{Q}{\kappa_{\text{drop}} A} z + T_{\text{memb}}, \quad \textbf{[S8]}$$

where, if we assume that droplet transfers heat across the contact (with height of t_{drop} and area of $\pi {R_{\text{drop}}}^2$) to a membrane, and that total power delivered to droplet is $Q \approx J_{\text{drop}} \pi {R_{\text{drop}}}^2 t_{\text{droplet}}$, we arrive at final expression that defines the temperature in terms of membrane, droplet properties, and beam conditions. The final expression for drop temperature is then

$$T_{\text{drop}} = T_0 + \frac{J_{\text{memb}} {R_b}^2}{2\kappa_{\text{memb}}}\ln(R_w/R_b) + \frac{J_{\text{memb}} {R_b}^2}{4\kappa_{\text{memb}}} + \frac{J_{\text{drop}} t_{\text{drop}} l_0}{\kappa_{\text{drop}}}. \quad \textbf{[S9]}$$

Fig. S7 plots the temperature change of the nanodroplet with respect to the ambient temperature ($\Delta T = T_{\text{drop}} - T_0$) as a function of electron beam flux for our experimental conditions [$T_0 = 293$ K, $R_w \approx 10$ μm, $R_b \approx 5$ μm, $\kappa_{\text{memb}} \approx 4.9$ W/(m·K), ref. 4, $\kappa_{\text{water}} \approx 0.6$ W/(m·K), $R_{\text{drop}} \approx 30$ nm, $t_{\text{droplet}} \approx 10$ nm, $l_0 \approx 0.37$ nm]. Therefore, TEM imaging doesn't result in substantial heating of the nanodroplets.

Convective flow of water. Based on our temperature estimates at the length scales of our nanodroplets, we will not have convective movement of water because the Rayleigh number defined as (5)

$$Ra = \frac{\alpha g \Delta T l^3}{\vartheta \mu} \approx 2 \times 10^{-17} \quad \textbf{[S10]}$$

is extremely small and we rule out the possibility of convection redistribution of water ($Ra > 10^3$ needed for convective flow to occur). Here, $\alpha = 2 \times 10^{-5}$ K^{-1} is the thermal expansion coefficient of water, $g = 9.8$ m/s^2 is the gravitational acceleration, $\Delta T = 0.1$ K is the possible temperature difference across the drop, $l = 50$ nm is the droplet length scale, $\nu = 1.4 \times 10^{-7}$ m^2/s is the thermal diffusivity of water, and $\mu = 9 \times 10^{-4}$ Pa·s is the water viscosity.

Temperature gradient. The temperature gradient is reported to induce the movement of the droplet (6). If we assume typical imaging conditions $n = 100$ e/(A^2·s) and that we are imaging at most halfway between the center of the beam and its edge ($0 < r < R_b/2$) of Eq. **S5**, we find the temperature radiant of a substrate with the nanodroplet

$$\frac{dT}{dr} = -\frac{J_{\text{memb}} r}{2\kappa_{\text{memb}}} < 1.6 \times 10^{-5} \text{ K/nm}. \quad \textbf{[S11]}$$

In order for a temperature gradient to induce a droplet movement, the contact angle hysteresis for a droplet movement on that surface, $\Delta\theta = \theta_{\text{adv}} - \theta_{\text{rec}}$, should satisfy the following condition (6):

$$\Delta\theta < R_{\text{drop}} \theta_c \frac{1}{\gamma}\frac{d\gamma}{dT}\frac{dT}{dr}. \quad \textbf{[S12]}$$

From a quick estimate for water (surface tension, $\gamma = 72$ mN/m; surface tension gradient, $d\gamma/dT \approx 0.2$ mN/(m·K); droplet radius, $R_{\text{drop}} = 25$ nm; critical angle, $\theta_c \sim 0.3$ rad) we find that contact angle hysteresis is $\Delta\theta < 3.4 \times 10^{-6}$ rad $\approx 2 \times 10^{-4}$°. This condition is practically impossible to satisfy even in recently fabricated ultralow contact angle hysteresis surfaces ($\Delta\theta > 1$°) (7, 8). Therefore, we safely rule out the possibility of temperature gradient induced movement of nanodroplets.

Nonuniform electron beam profile may potentially be a source for temperature gradient, but our beam is considerably uniform (Fig. S8).

Possible Role of Electron Beam-Induced Radiation Pressure on Droplet Deformation. To consider the effect of the radiation pressure exerted by electron beam on a specimen that is being imaged due to electron scattering, we need to consider only the fraction of the electrons that are scattered, which is given by

$$\frac{N_{\text{scat}}}{N_{\text{tot}}} = 1 - \exp(-t/\lambda), \quad \textbf{[S13]}$$

where N_{scat} is the number of scattered electrons, N_{tot} is total number of electrons impacting the sample, t is specimen thickness, and λ is mean free path of the 120-keV energy electron in water.

The momentum change, Δp, of each scattered electron during the time interval, Δt, when an electron interacts with the sample is $\Delta p = p(1 - \cos\theta) = (2m_e E)^{1/2}(1 - \cos\theta)$, where we have neglected relativistic effects for simplicity. This momentum change exerts a force and therefore a pressure on a sample area of A:

$$\begin{aligned} P &= \frac{F}{A} = \frac{1}{A}\frac{N_{\text{scat}}\Delta p}{\Delta t} = \frac{N_{\text{scat}}}{A\Delta t}\sqrt{2m_e E}(1 - \overline{\cos\theta}) \\ &= \frac{N_{\text{tot}}}{A\Delta t}(1 - \exp(-t/\lambda))\sqrt{2m_e E}(1 - \overline{\cos\theta}), \end{aligned} \quad \textbf{[S14]}$$

where θ is the scattering angle (usually a few degrees), $m_e = 9.1 \times 10^{-31}$ kg is the mass of the electron, and $E = 120$ keV is the energy of the electron. If we assume that electrons undergo complete backward scattering ($\theta = 180$°) which yields the maximum possible pressure, we calculate a pressure of 0.31 Pa, which is negligible compared to Laplace pressure inside the nanodroplet:

$$P = \frac{\gamma}{R} = 2.9 \text{ MPa}.$$

Here we used known values of $\gamma = 0.072$ N/m, $m_e = 9.1 \times 10^{-31}$ kg, $E = 120$ keV, $(\frac{N_{tot}}{A\Delta t}) = 100$ electrons/(A^2·s) – typical experimental values, $t \approx 20$ nm, $\lambda = 232$ nm (9), $R = 25$ nm. Therefore, we conclude that it is unlikely that radiation pressure will induce any noticeable deformation of the nanodroplet.

Possible Role of Electrostatic Forces in Deformation of the Nanodroplet. Electrostatic effects may also deform the nanodroplets. We can model the nanodroplet of radius R to be a spherical capacitor with the capacitance of $C = 4\pi\varepsilon_0 R$ that charges up with charge q when exposed to energetic electron beam as a result of ionization ($\varepsilon_0 = 8.85 \times 10^{-12}$ F/m). The energy stored in this nanodroplet capacitor is then $E = q^2/2C$. In order for the electrostatic energy to induce a deformation, it should be comparable to the surface energy of the nanodroplet, $E = \gamma A = 4\gamma\pi R^2$, where $A = \pi R^2$ is the surface area of the sphere. Setting electrostatic energy equal to the surface energy of the nanodroplet ($R = 25$ nm), we obtain total charge necessary to induce the deformation of

$$q = 4\pi(2\varepsilon_0\gamma R^3)^{1/2} = 350e.$$

Nanodroplet with a radius of 25 nm contains about 2.2×10^7 water molecules. Such ionization of a very small fraction of water molecules ($350/2.2 \times 10^7 = 0.0016\%$) can lead to internal electrostatic repulsive force that results in toroidal shape as water is pushed toward the rims of the nanodroplet, leading to an increase in contact angle until the advancing contact angle is reached. As the droplet steps forward it may lose some outward charge diffusion (to membrane and air interface) and because of the enlarged total area, which will reduce the overall charge of the droplet as it comes to rest and this cycle repeats, forcing the nanodroplet to undergo stick-slip movement.

1. Masahide G, Masao W (2005) Self-propulsion of a water droplet in an electric field. *J Phys D Appl Phys* 38:2417.
2. Martin B (2009) *Nuclear and Particle Physics* (Wiley, Chichester, UK), pp 122–124.
3. Zheng H, et al. (2011) Observation of transient structural-transformation dynamics in a Cu2S nanorod. *Science* 333:206–209.
4. Jain A, Goodson KE (2008) Measurement of the thermal conductivity and heat capacity of freestanding shape memory thin films using the 3 omega method. *J Heat Trans* 130:102402.
5. Linden PF (2000) *Perspectives in Fluid Dynamics: A Collective Introduction to Current Research*, eds. Batchelor GK, Moffatt HK, Worster MG (Cambridge Univ Press, Cambridge, UK), pp 289–294.
6. Brzoska JB, Brochard-Wyart F, Rondelez F (1993) Motions of droplets on hydrophobic model surfaces induced by thermal gradients. *Langmuir* 9:2220–2224.
7. Won T-S, et al. (2011) Bioinspired self-repairing slippery surfaces with pressure-stable omniphobicity. *Nature* 477:443–447.
8. Lee S, Hwang W (2009) Ultralow contact angle hysteresis and no-aging effects in superhydrophobic tangled nanofiber structures generated by controlling the pore size of a 99.5% aluminum foil. *J Micromech Microeng* 19:035019.
9. Feja B, Aebi U (1999) Determination of the inelastic mean free path of electrons in vitrified ice layers for on-line thickness measurements by zero-loss imaging. *J Microsc* 193:15–19.

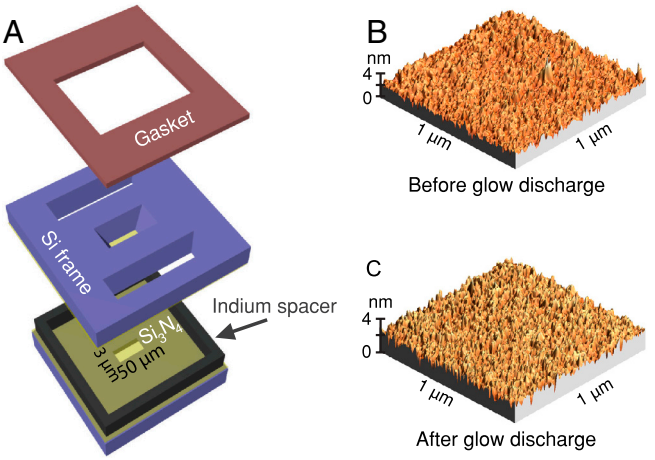

Fig. S1. The liquid cell. (*A*) Si_3N_4 membrane windows both on top and bottom frame are aligned and attached together with indium spacer providing a gap for liquid to be loaded from two large openings at the top of the chip. Once liquid is loaded, the chip is sealed by a copper gasket that prevents the liquid from being exposed to vacuum of TEM. Surface topography of Si_3N_4 membrane window (*B*) before and (*C*) after glow discharge.

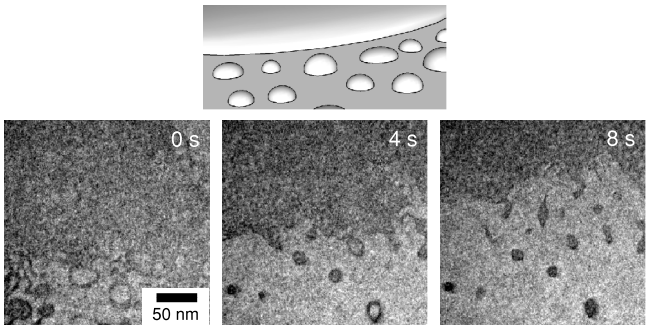

Fig. S2. Water nanodroplet formation. TEM micrograph showing the droplet formation as thin water film recedes when exposed to an electron beam with flux of >120 e/(A^2·s).

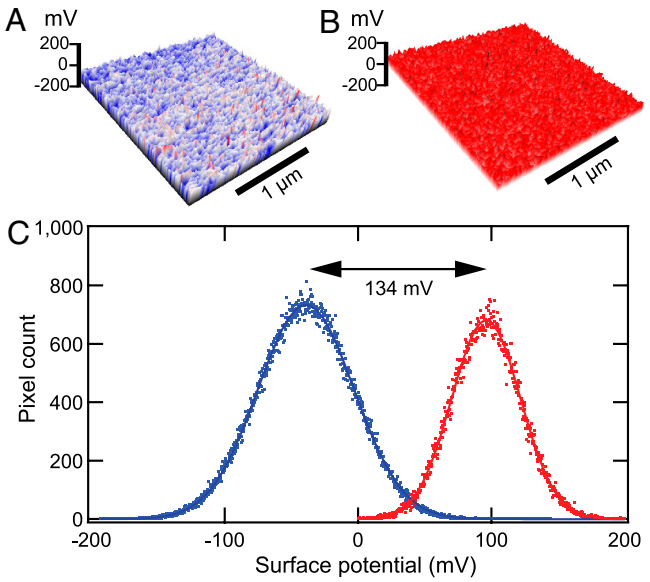

Fig. S3. Influence of electron beam on the surface potential of the membrane obtained by scanning kelvin probe microscopy. (*A*) Prior to an electron beam exposure. (*B*) After the exposure to an electron beam (approximately 60 $e/Å^2 \cdot s$ for duration of approximately 4 min; measured approximately 60 min after electron beam exposure). (*C*) Histogram of voltage distribution of Si_3N_4 before (blue) and after (red) the electron beam exposure obtained from 512×512 pixel scanning kelvin probe micrographs.

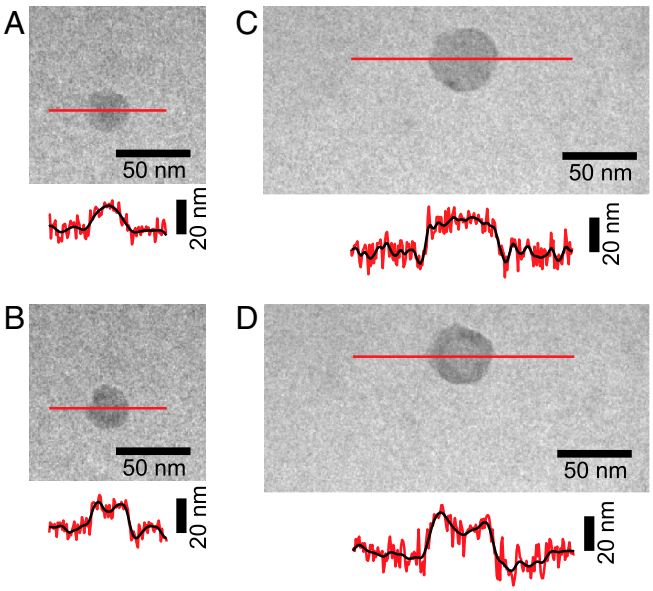

Fig. S4. Estimating the rough thickness of a nanodroplet. (*A*) Thickness of a stationary 30-nm water droplet. (*B*) Thickness as 30-nm droplet prepares to step by forming a torus structure. (*C*) Thickness of a stationary 60-nm water droplet. (*D*) Thickness as 60-nm droplet prepares to step by forming a torus.

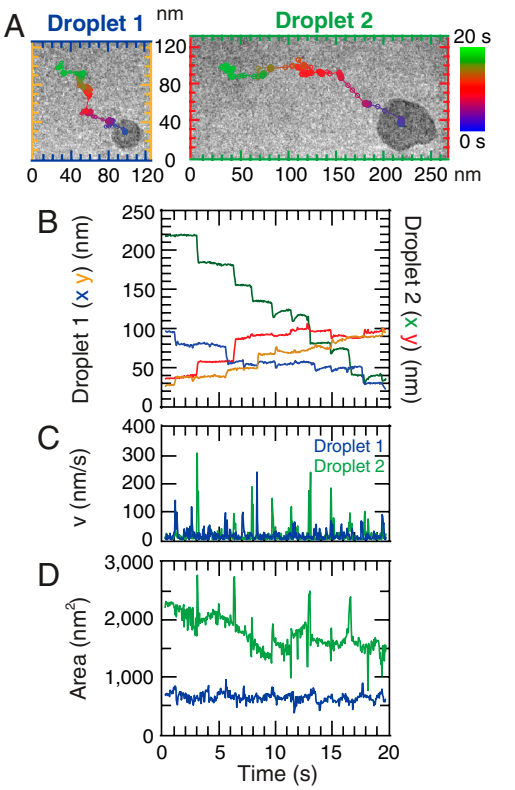

Fig. S5. Nanodroplet parameters. (*A*) Droplet 1 and droplet 2. (*B*) Coordinates *x*-*y* of two droplets. (*C*) Instantaneous velocities of the droplet 1 (blue) and droplet 2 (green). (*D*) Area of the droplet 1 (blue) and droplet 2 (green).

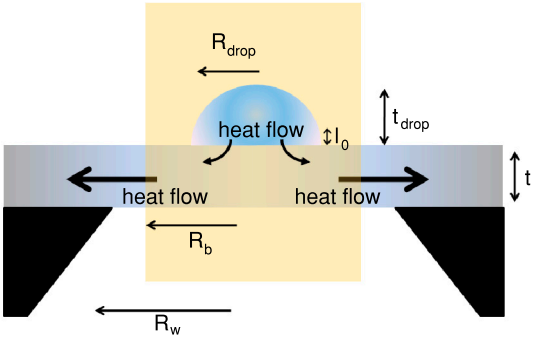

Fig. S6. Schematic of droplet under e-beam. Electron beam (yellow region) interacts both with the substrate and freestanding Si_3N_4 membrane. Absorbed energy from droplet dissipates into the membrane, while the energy input into membrane dissipates to thick Si frame of the chip, which is in direct contact with the specimen holder.

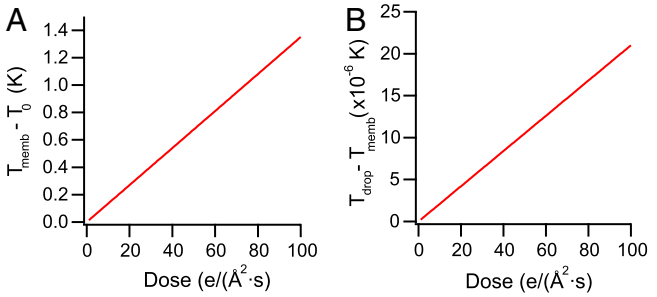

Fig. S7. Estimated temperature dependence on electron dose. (*A*) Temperature difference between the membrane and the ambient environment due to the electron beam. (*B*) The difference between the nanodroplet and the membrane temperature in the presence of the 120 keV electron beam.

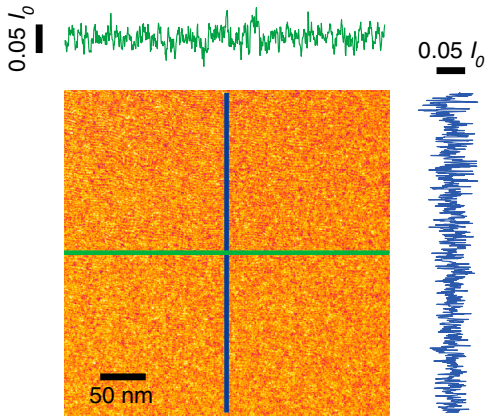

Fig. S8. Typical beam profile used during imaging of droplet movement recorded by camera appears to be considerably flat (within 5% of incident beam intensity).

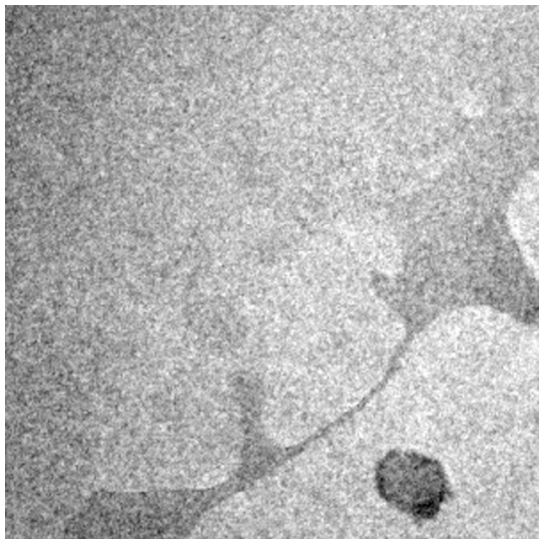

Movie S1. Movie of water film flowing back and rewetting the membrane surface after beam was turned off for a few minutes.

Movie S1 (MOV)

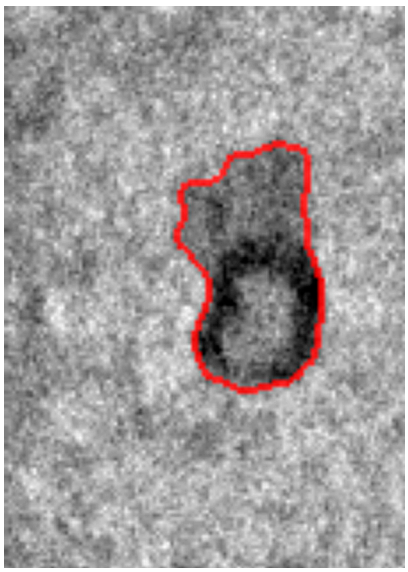

Movie S2. Movie of a approximately 50-nm nanodroplet (red outline) executing stick-slip movement on a flat Si_3N_4 film imaged with electron flux of 52 e/(Å^2·s).

Movie S2 (MOV)

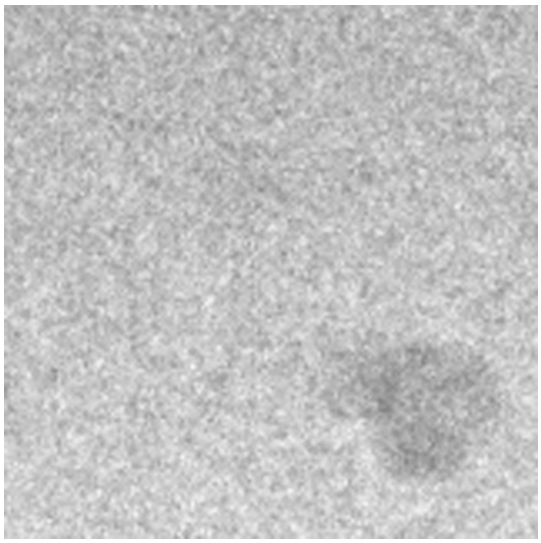

Movie S3. Movie of an approximately 30-nm nanodroplet executing stick-slip movement on a flat Si_3N_4 film imaged with electron flux of 95 e/(Å^2·s).

Movie S3 (MOV)

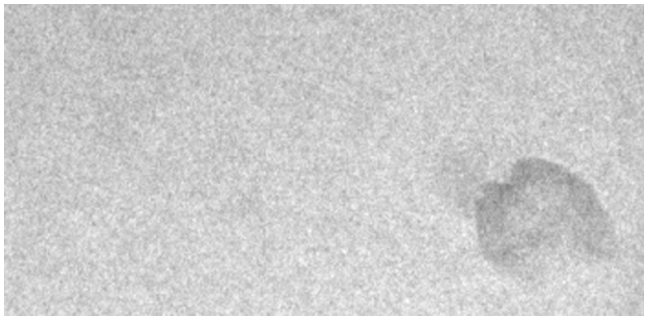

Movie S4. Movie of an approximately 60-nm nanodroplet executing stick-slip movement on a flat Si_3N_4 film imaged with electron flux of 95 e/(Å^2·s).

Movie S4 (AVI)

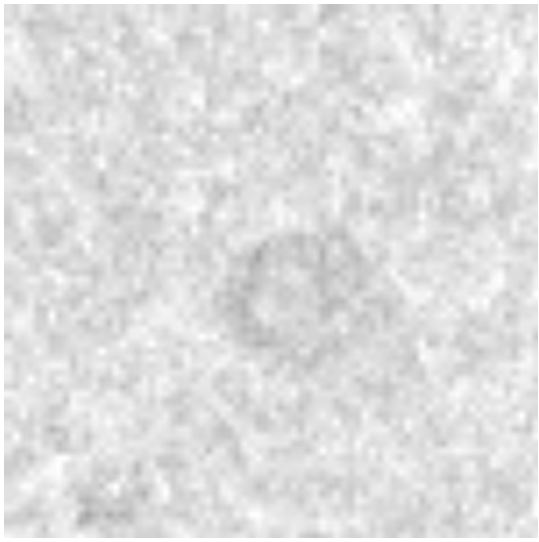

Movie S5. Movie of an approximately 15-nm nanodroplet executing attempting stick-slip movement on a flat Si_3N_4 film imaged with electron flux of 95 e/(Å^2·s). However, the droplet remains pinned to the surface and immobile.

Movie S5 (MOV)